Published in: Acta biomaterialia (2005), vol. 1, iss. 5, pp. 565-574
Status: Postprint (Author's version)

Study of the connectivity properties of Bioglass®-filled polylactide foam scaffolds by image analysis and impedance spectroscopy

S. Blacher [a], V. Maquet [b] , R. Jérôme [b] , J.-P. Pirard [a], A.R. Boccaccini [c]

[a] Department of Chemical Engineering, University of Liège, B-4000 Liège, Belgium
[b] Centre for Education and Research on Macromolecules (CERM), University of Liège, B-4000 Liège, Belgium
[c] Department of Materials and Centre for Tissue Engineering and Regenerative Medicine, Imperial College London, London SW7 2BP, UK

Abstract: The porous structure of two series of poly(D , L -lactide)/Bioglass® composite foams prepared by thermal-induced phase separation was investigated by image analysis and impedance spectroscopy. Polymer solutions of either low or high molecular weight containing different concentrations (up to 50 wt.%) of Bioglass® particles of mean particle size $d < 5$ μm were studied. The morphology of both macro- and micropores was studied by scanning electron microscopy and image analysis of both neat and composite foams (containing 10-50 wt.% Bioglass®). The pore connectivity of both neat polymer and composite foams was characterized by impedance spectroscopy in relation with their transport properties. The influence of the foam composition (i.e., polymer molecular weight and concentration of Bioglass®) on pore microstructure was studied using these non-destructive methods. It was found that addition of Bioglass® particles has a pronounced effect on pore orientation, leading to increasing loss of order of pore structure, especially for low-molecular weight PDLLA foams.

Keywords: Composite foams; Impedance spectroscopy; Image analysis; Porous scaffolds

1. INTRODUCTION

Manufacture of polymer scaffolds for tissue engineering applications has been extensively investigated to aid the design of living substitutes for lost or damaged tissue and organs [1,2]. Biodegradable polymer scaffolds are intended to provide cells with a biological and phys-ico-mechanical environment analog to the native extra cellular matrix, in order to trigger cell attachment, growth and expansion. The accurate characterization of the porous structure of scaffolds represents a fundamental requisite for scaffold optimization for different applications. Recently, some of us reported on the use of non-destructive methods in order to investigate the texture of highly porous polylactide foams with complex 3-D morphologies and/or fragile mechanical properties [3]. A methodology based on image analysis and impedance spectroscopy has been developed to collect information on the pore structure and connectivity. These data are complementary to results obtained using mercury intrusion porosimetry and are more reliable in case of fragile foams. The same methodology also proved to be valuable to quantify cellular parameters and to gain more insight into the relationships between pore structure and cell colonization of polymer scaffolds intended for nerve regeneration [4].

In this paper, image analysis and impedance spectroscopy have been applied in order to analyze the micro-structure of polymer/Bioglass® composite foams which are being developed for bone tissue engineering scaffolds [5]. The preparation by thermally induced phase separation (TIPS) and the qualitative microstructural characterization of polymer/Bioglass® composite foams made of biodegradable poly(α-hydroxyacids) including poly(D,L-lactide) and poly(lactide-co-glycolide) have been previously described [5]. Such composites hold great promise for bone tissue engineering because of the benefits of the Bioglass filler, which endowed polymer foams with osteoinductive properties. However, there has been no previous study on the quantitative correlation between composite foam composition, processing parameters and porosity structure. In order to fill this gap of understanding, in particular to gain more (quantitative) insight into the influence of different concentrations of Bioglass® inclusions on the resultant pore structure of TIPS processed foams, image analysis and impedance spectroscopy have been applied in this study.

Published in: Acta biomaterialia (2005), vol. 1, iss. 5, pp. 565-574
Status: Postprint (Author's version)

2. MATERIALS AND METHODS

2.1. Polymer/Bioglass® foams

Foams were prepared using Purasorb poly(D , L -lac-tide) (PDLLA) from Purac biochem (Goerinchen, The Netherlands) with two inherent viscosities (i.v.): (a) PDLLA with i.v. = 0.39 dl/g, a low molecular weight polymer (PDLLA-LMW) and (b) PDLLA with i.v. = 1.52 dl/g, a high molecular weight polymer (PDLLA-HMW). Dimethylcarbonate (DMC) of 99% purity (Sigma Aldrich) was used as a solvent for freeze-drying of polymer solutions and preparation of foams by TIPS [5]. The bioactive material used in all composites was a melt-derived bioactive glass powder (Bioglass® grade 45S5). The powder had a mean particle size <5 μm. The composition of the bioactive glass used was (in weight percentage): 45% SiO_2, 24.5% Na_2O, 24.5% CaO and 6% P_2O_5, which is the original composition of the first bioactive glass developed by Hench et al. [6]. Neat polymer and composite foams were prepared by the thermally induced phase separation process (TIPS), as described in our previous publications [5,7]. Composite foams were prepared as follows: the polymer was dissolved in DMC by magnetic stirring to produce a polymer weight to solvent volume ratio of 5% (w/v). A given amount of 45S5 Bioglass® powder was added into the polymer solution and sonicated for 15 min to improve the dispersion of the glass particles into the polymer solution. This dispersion was then quenched by immersion of the flask into liquid nitrogen (—196 °C) for 2 h. The flask was then transferred into a ethylengly-col bath at —10 °C and the solvent was removed from the frozen mixture by vacuum sublimation at 10^{-2} Torr (by connection to a vacuum pump). Solvent sublimation was carried out at —10 °C for 48 h and then at 0 °C for 48 h. The sample was then transferred in a vacuum oven for final drying at room temperature until reaching a constant weight. Two series of composites foams were prepared composed of PDLLA-LMW or PDLLA-HMW filled with 0, 10, 25 and 50 wt.% of Bioglass® particles. Neat polymer foams were prepared using the same processing method in the absence of Bioglass . Such foams have been previously characterized for their apparent density and porosity [7]. The results of these measurement showed that in HMW-PDLLA foams the apparent density was increased from 0.10 to 0.17 g/cm^3 when the Bioglass® content was increased up to 40 wt.%, leading to a decrease of pore volume from 9.5 to 5.7 cm^3/g [7]. The same tendency also prevailed for the LMW-PDLLA foams. However, in comparison with HMW-PDLLA foams, foams made from LMW-PDLLA and the same Bioglass® content were less dense (or more porous); the apparent density increasing from 0.08 to 0.11 g/cm^3 when the Bioglass® content was increased up to 50%.

2.2. Scanning electron microscopy and image analysis

At least five representative samples were cut out of the as-prepared foams using a razor blade. Longitudinal and transverse sections were obtained by cutting the foams in direction parallel and perpendicular to the surface. Samples were observed using a Jeol JSM-840A scanning electron microscope (SEM) at an accelerating voltage of 20 kV. SEM micrographs magnified x30 and x100, respectively, allowed the macropores (ca. 100 μm width) and the micropores (10-50 μm width) to be discriminated properly. Image analysis was performed using the software Visilog 5.4 (Neosis).

In order to quantify the pore orientation from SEM images, preliminary gray level image transformations are necessary to improve the quality of the image. This transformation is followed by a segmentation step consisting in the transformation of the gray level image into a binary image in which the intensity of the pixels is 1 on the polymer (white on the images) and 0 in the pores (black on the image). To achieve this goal, the following algorithm based on traditional tools of signal processing and of mathematical morphology [8] was used: (a) enhancement of local pore edges by the gradient technique, (b) threshold transformation in order to binarize the images, (c) opening transformation with segments oriented in the main direction of the pore edges in order to eliminate artifacts, (d) image reconstruction from open image markers. A similar algorithm was used in the previous studies on similar foams [3,4]. As an example of the application of this image analysis procedure, Fig. 1a and b show the original SEM micrographs of longitudinal cross sections at magnification x100 of neat PDLLA-LMW and PDLLA-LMW foams filled with 50 wt.% Bioglass® particles, and Fig. 1c and d are the corresponding binary images.

***Fig. 1**. Image analysis processing: Original SEM images at x100 magnification of (a) neat PDLLA-LMW and (b) neat PDLLA-HMW foams and the corresponding binary processed images (c) and (d).*

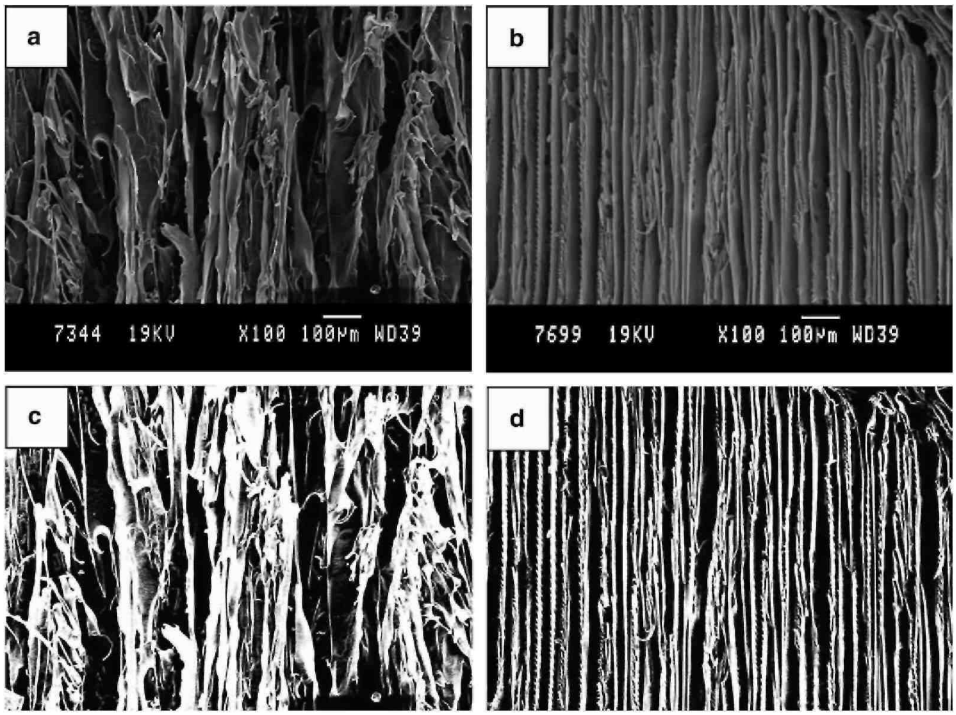

From binary images, orientations are quantified using a rose of directions [8], which allows characterizing the directional structure of contours or line sets. The rose is defined as the density of the contour length *L* as a function of the non-oriented tangent direction α (between 0 and *π), ΔL/Δα = R(α),* where *R(α)* corresponds to the contribution to the contour of all arcs with direction in the interval Δα. Practically, *R(α)* is estimated by the relation *R(α) = D(α) + D″(α),* where *D(α)* is the diametral variation or intercept defined as the number of entries in an object along a given direction and *D″(α)* is the sec-ond order derivative of *D(α).* Taking into account that an image consists of a network of points distributed on a discrete hexagonal grid, the estimation of D(α) in directions that are not aligned with the grid is a difficult task. Therefore D(α) is calculated only for the main directions of the rotated grids. The second order derivative is computed by adjusting a parabolic function to the measured distribution D(α). The resulting measure, is the total number of segments in the image in the directions 0°, 30°, 60°, 90°, 120° and 150°. The mean values for each direction, obtained averaging at least five images are further represented in a normalized histogram together with the respective standard deviations.

2.3. Impedance spectroscopy

Impedance spectroscopy measurements were per-formed using a Schlumberger SI 1255 frequency analyzer (Chelsea Dielectric Interface (Model CDI 4t)). Alternative current with constant voltage (0.1 V) was applied with a frequency range of 10^{-3} -10^{6} Hz. Cubic-shape samples (10 **x** 10 **x** 10 mm^3) were cut out of the foams. The non-porous skin, which is usually observed at the top surface of foams prepared using the freeze-drying process, was removed prior to measurement. The sample was placed in an UV cell between two parallel stainless-steel electrodes. This cell was filled with freshly deionized water. Prior to the measurements, each foam sample was degassed for 30 min in freshly deionized water.

3. RESULTS

3.1. Porous morphology by scanning electron microscopy and image analysis

In order to determine the influence of Bioglass® concentration on the pore morphology of polymer/Bioglass® composite foams, two series of foams prepared by adding different weight percentage of Bioglass par-ticles to low and high molecular weight PDLLA foams were investigated.

Typical SEM micrographs for PDLLA-LMW and PDLLA-HMW foams (without Bioglass®) and composites foams containing 10 and 50 wt.% Bioglass® are shown in Figs. 2 and 3, respectively. For comparison with previous studies [3,4], pores observed at x30 and x100 magnification will be referred as macro- and micropores,

respectively. In low MW PDLLA foams, for a given Bioglass® concentration, transversal SEM micrographs show a similar structure whatever the magnification used, i.e., x30 or x100 (Fig. 2). Indeed, these foams exhibit a disordered structure, the pores being rather elongated with a rough surface. The structure of the composite foams containing 50 wt.% Bioglass® was even more disordered, to the point that there was no more structural difference between longitudinal and transversal sections (Fig. 2h and i). Longitudinal sections shown in Fig. 2g-i show that pores in PDLLA-LMW foams without Bioglass® were poorly oriented and that addition of Bioglass® seems to have limited effect on this parameter. SEM micrographs of transverse sections of neat PDLLA-HMW foams observed at low magnification exhibit a bimodal porous structure with macropores of ~100 μm diameter and almost circular shape, coexisting with micropores (Fig. 3a). Longitudinal sections observed at a x100 magnification show that pores are properly oriented along the longitudinal direction, as a result of the unidirectional cooling process (Fig. 3c). This pore orientation was preserved for foams filled with 10 wt.% of Bioglass® particles whereas upon addition of higher concentration of Bioglass® the structure became much less organized and mainly shapeless pores were detected (Fig. 3i). However, the longitudinal orientation of pores was still observed.

In order to quantify the degree and direction of pore orientation, the histogram of orientations was calculated from longitudinal section images obtained at 100x magnification, for neat and filled PDLLA-LMW and PDLLA-HMW foams. The results are shown in Fig. 4a and b. For both neat foams, a peak at orientation 90° is observed indicating that most pores have a defined orientation. However, comparison between the heights of those peaks indicates that the normalized frequency of oriented pores is 1.5 larger for the PDLLA-HMW foams. Moreover the histograms of orientations show that the differences between pore orientations of neat PDLLA-LMW and Bioglass filled PDLLA-LMW foams are not significant. On the contrary, for PDLLA-HMW foams, no significant difference is observed between neat and 10 wt.% Bioglass® filled foams whereas pores are significantly less orientated in foams with higher Bioglass® content.

Fig. 2. *SEM micrographs of transversal sections at magnification x30 of PDLLA-LMW foams: (a) neat, (b) filled with 10 wt.% and (c) filled with 50 wt.% Bioglass particles. SEM micrographs of transversal sections at magnification x100 of PDLLA-LMW foams: (d) neat, (e) filled with 10 wt.% and (f) filled with 50 wt.% Bioglass particles. SEM micrographs of longitudinal sections at magnification x100 of PDLLA-LMW foams: (g) neat, (h) filled with 10 wt.% and (i) filled with 50 wt.% Bioglass® particles.*

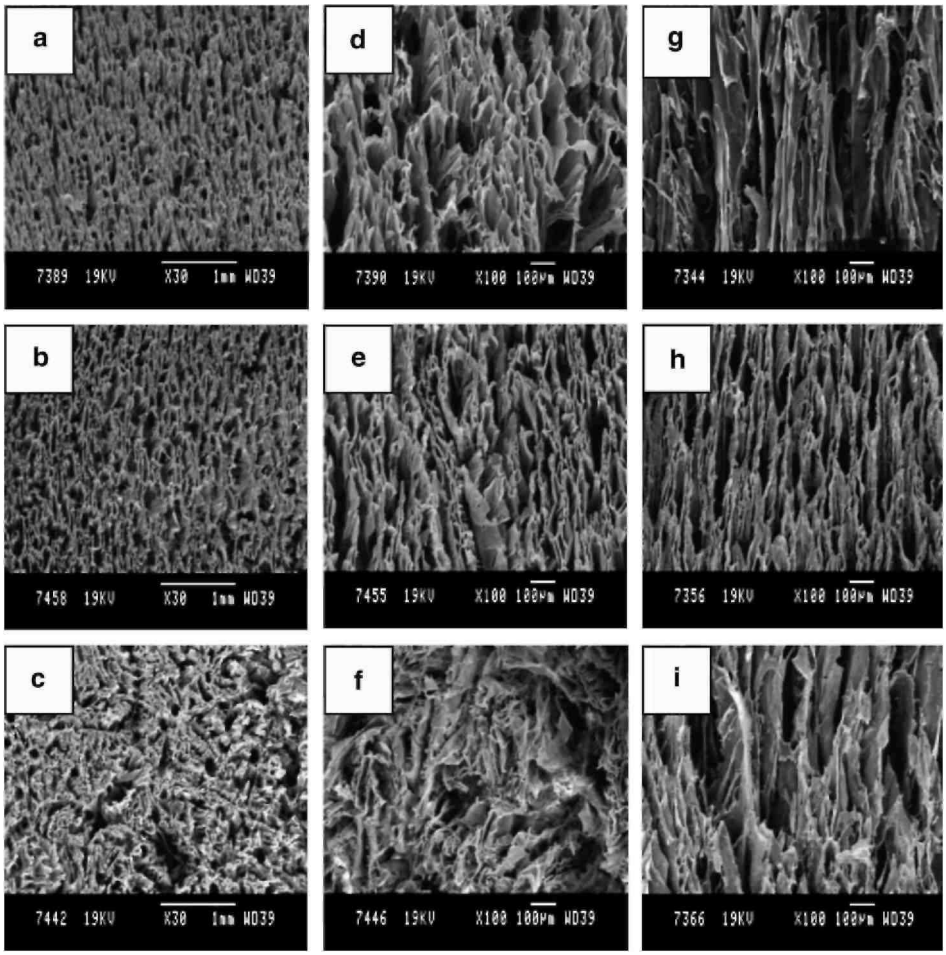

Fig. 3. *SEM micrographs of transversal sections at magnification x30 of PDLLA-HMW foams: (a) neat, (b) filled with 10 wt.% and (c) filled with 50 wt.% Bioglass® particles. SEM micrographs of transversal sections at magnification x100 of PDLLA-HMW foams: (d) neat, (e) filled with 10 wt.% and (f) filled with 50 wt.% Bioglass® particles. SEM micrographs of longitudinal sections at magnification x100 of PDLLA-HMW foams: (g) neat, (h) filled with 10 wt.% and (i) filled with 50 wt.% Bioglass® particles.*

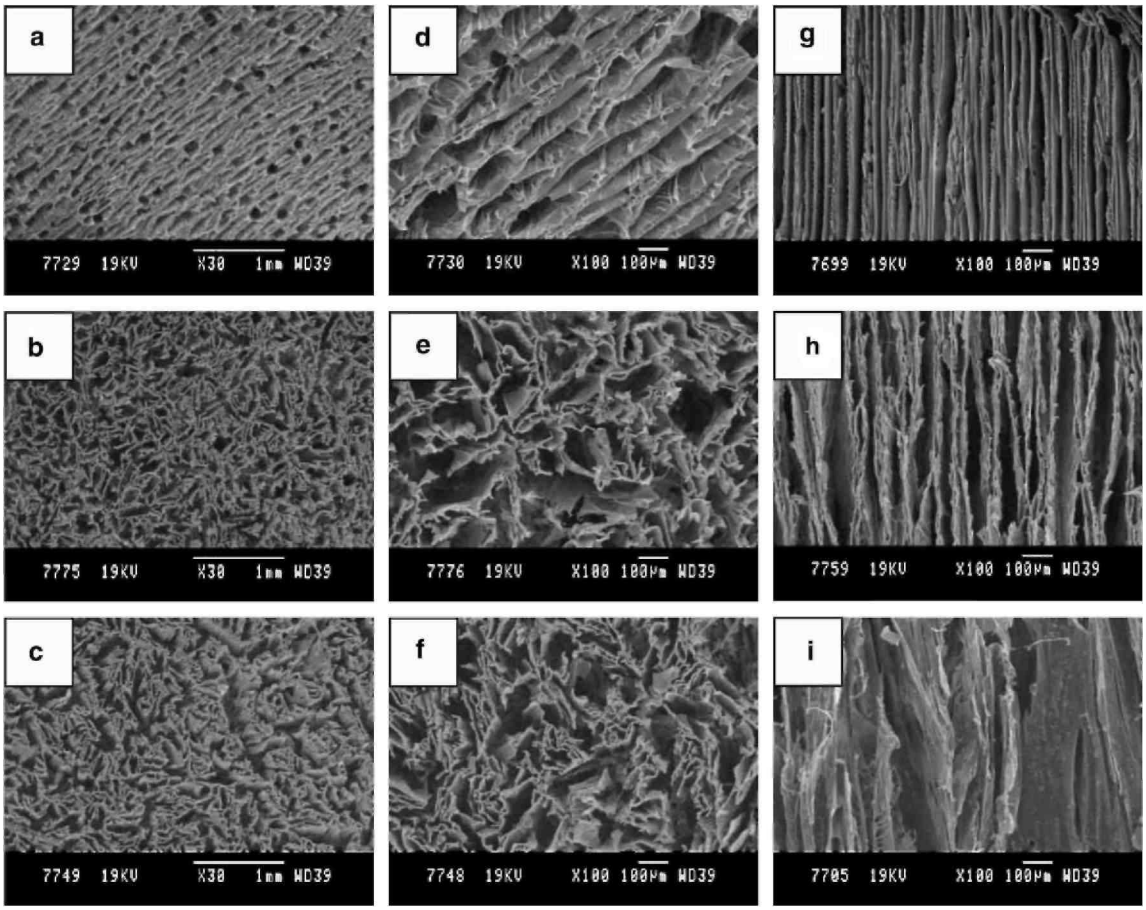

3.2. Dielectric properties

The conducting properties of a porous medium saturated with a liquid can provide information on pore geometry and on pore surface area [9]. Indeed, both the motion of free carriers and the polarization of the pore interfaces contribute to the total conductivity. The main studies in this field deal with the frequency dependence of conductivity for water or brine-saturated rocks [9] as well as porous glasses [10-12]. Dielectric properties are usually expressed by the frequency-dependent real and imaginary components of the complex dielectric permittivity (ε*):

$$\varepsilon^*(\omega) = \varepsilon'(\omega) - i\varepsilon''(\omega) = \varepsilon'(\omega)\varepsilon_0 - \frac{i\sigma'(w)}{\omega} \quad (1)$$

where $i = v\sqrt{-1}$, ε_0 is the dielectric permittivity of vacuum, $\omega = 2\pi f$, with f the frequency in hertz, ε' is the dielectric constant, ε'' is the conductance and σ' is the conductivity. Experimental data are usually shown as a log-log plot of ε' and ε'' against frequency. Alternatively, ε' can be plotted against ε'', which is referred to as the Cole-Cole plot [13]. Several models have been proposed to interpret the frequency dependence of the permittivity data. The first one, proposed by Debye [14], considers an almost ideal situation with a single relaxation time (τ). The permittivity is then expressed as $\varepsilon^* = \varepsilon_\infty + \frac{\varepsilon_0 - \varepsilon_\infty}{1 + i\omega\tau'}$ where ε_s and ε_∞ are, respectively, the dc and the infinite frequency dielectric constant. In a Debye process, a maximum in ε'' is observed at $f = (2\pi\tau)^{-1}$ in a log-log plot of ε'' vs. f. In a Cole-Cole plot, a semicircle centred on the real axis is the Debye response. In an attempt to approach real systems, Cole and Cole [13] introduced an empirical parameter

(α) in the Debye equation, according to the equation $\varepsilon^* = \varepsilon_\infty + \frac{\varepsilon_0 - \varepsilon_\infty}{1+(i\omega\tau)^{1-\alpha}}$. This equation accounts for a distribution

of the relaxation times and results in a depressed semicircle in the Cole-Cole plot. Alternative empirical fittings [15,16] and additional theoretical models [17,18] are also available. In a different approach, Jonscher [19] suggested, on the basis of experimental evidence, that the dielectric response of any dielectric solid agrees with a fractional power-law $\varepsilon^* \alpha (i\omega)^{n-1}$, with $0 < n < 1$. Recently, some of us used the dielectric response of water-saturated freeze-dried polymer matrices to extract information about their three-dimensional internal structure [3,4]. Freeze-dried porous polymer matrices are three-dimensional isolating solids consisting of a more or less oriented micro- and macropore network, through which ionic species can migrate depending on the network structure.

***Fig. 4**. Histograms of pore orientations for (a) PDLLA-LMW foams and (b) PDLLA-HMW foams.*

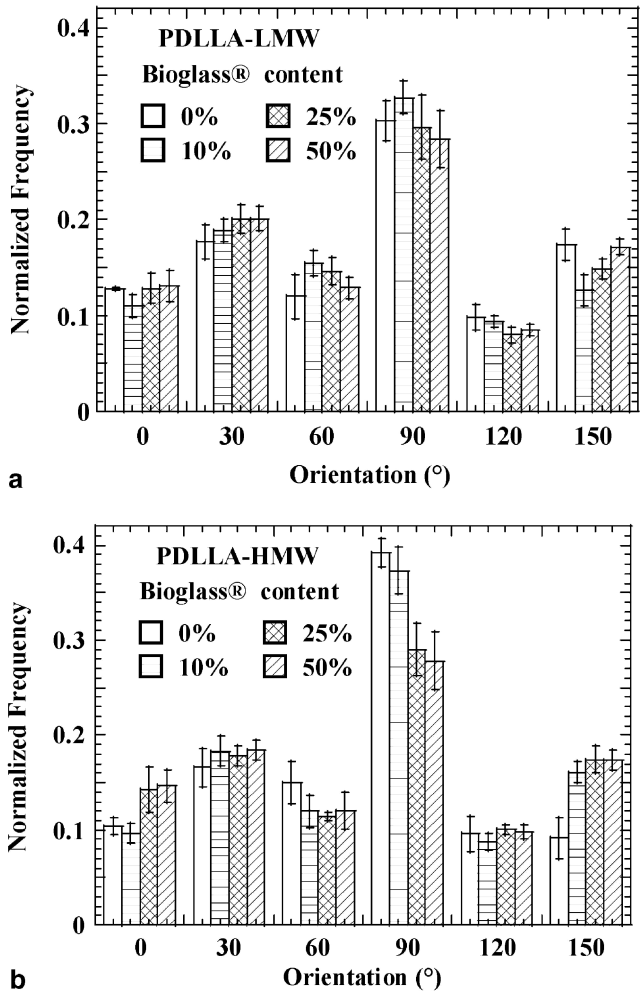

For the first time the technique has been used in the present investigation to characterise the pore structure of PDLLA-Bioglass® composite foams.

Fig. 5a-d show plots of ε" and ε'asa function of the frequency for PDLLA-LMW and PDLLA-HMW foams prepared with various concentrations of Bio-glass® (0 wt.%, 10wt.%, 25 wt.% and 50wt.%). The electrodes were placed in the longitudinal direction of pores. At frequencies higher than ~10^{-1} Hz, the data agree with the Cole-Cole behaviour, i.e., $\varepsilon'' \alpha \omega^{-1}$ and $\varepsilon' \alpha \omega^{-2}$, in all cases but in an interval of frequency which depends of the Bioglass® content. At low frequencies ε' tends to a plateau, as well as ε''. For high Bioglass® contents an incipient loss peak is visible in e particularly for PDLLA-HMW.

It must be noticed that the permittivity depends on both foam composition, i.e., polymer molecular weight, and Bioglass® content. Taking into account that all samples are impregnated with the same quantity of water, the polymer should released a certain amount of ions (due to hydrolytic degradation) leading to an increase of the

permittivity as compared to that of pure water. Moreover, additional charge carriers could also be released from the Bioglass® particles which explain the increase of the conductance with the concentration of Bioglass® particles. Although the real mechanism of conduction in these porous composites has not been deeply investigated, this feature has also been observed in previous investigations on similar polymer foams [3,4].

A more straightforward interpretation of the impedance spectroscopy data is obtained by plotting the ionic conductivity σ' versus frequency in logarithmic scale. In this representation, a conducting system leads to an horizontal line, wherein σ' is independent of the frequency, whereas an isolating system leads to $\sigma' = \omega$. Fig. 6a and b show the ionic conduction curves of PDLLA-LMW and PDLLA-HMW impregnated foams, respectively. The curves corresponding to the pure deionized water and the impregnated foams of various compositions were rescaled and plotted on the same figure for comparison purposes.

For the two series of foams, the size of the conductivity plateau, corresponding to the interval of frequencies in which the system is conducting, depends of the foam composition. The conductivity profile of the PDLLA-LMW neat foam is very close to that of the deionized water indicating ''free'' charge motion within this porous material. For the PDLLA-LMW composite foams containing Bioglass® (Fig. 5a), the size of the conductivity plateau decreases gradually with Bioglass® content, indicating loss of ionic conductivity. For PDLLA-HMW foams (Fig. 5b), the ionic conductivity of the neat polymer foam increases in a narrower frequency interval than that of pure water. The size of this interval further drastically decreases for higher Bioglass® content (10-50 wt.%). Therefore, it is found that the dielectric behaviour of the neat PDLLA-HMW polymer foams is intermediate between that of pure water and that of the PDLLA/Bioglass® composite foams (with 10-50 wt.% Bioglass content). This result indicates that the higher the Bioglass® content, the more the charge carriers are hindered in their motion over extended regions in the foams.

Fig. 5. *Log-log plots of (a,c) the dielectric constant (**ε'**) and (b,d) the conductance (**ε''**) versus frequency for PDLLA-LMW and PDLLA-HMW foams unfilled and filled with different concentrations of Bioglass®.*

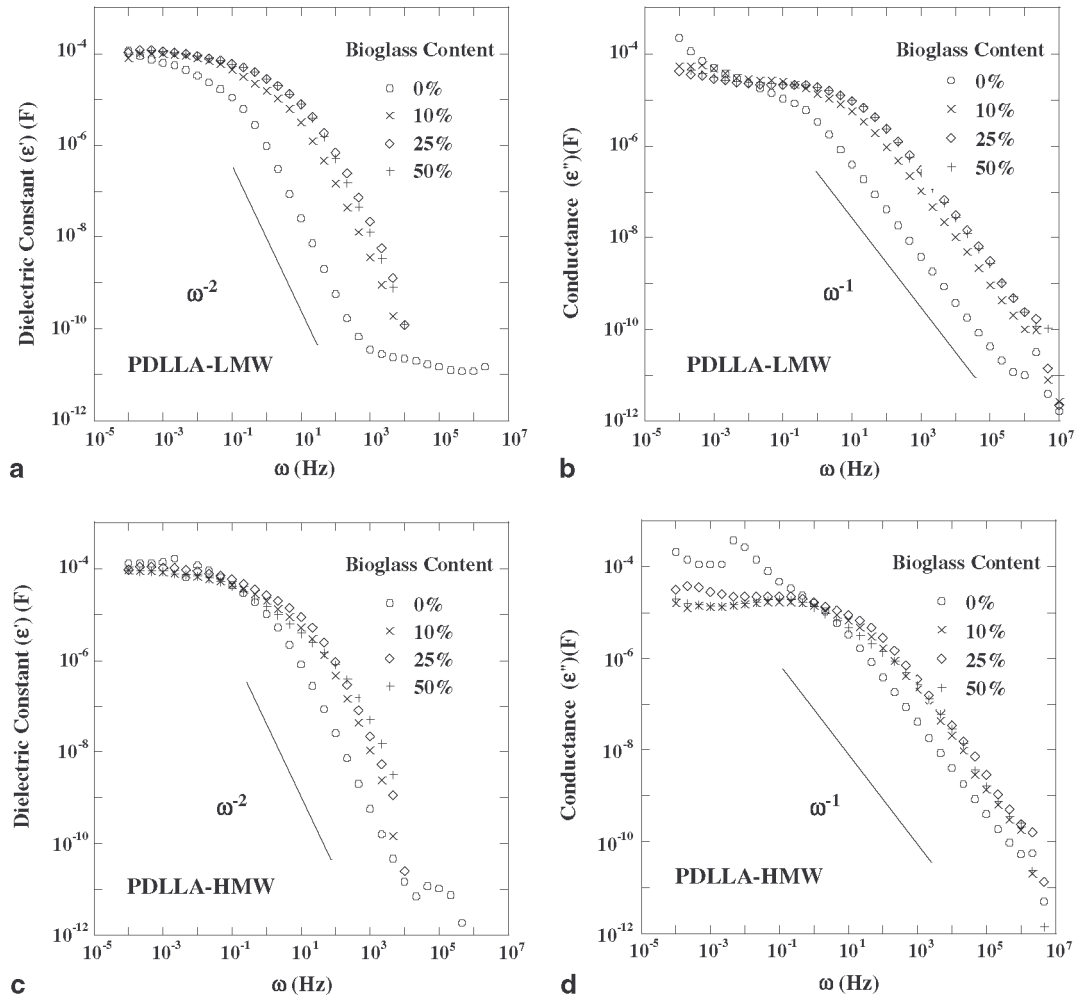

In order to quantify the difference between the conducting behaviour of the different foams, conductivity data have been fitted using the following empirical relation:

$$\sigma(\omega)\alpha\frac{(\omega/\omega_1)^{\alpha}}{1+(\omega/\omega_2)^{\alpha}} \qquad (2)$$

where for ω —> 0, σ α ω, for ω —> ∞, $\sigma = \sigma_c$ and α is a constant. In this expression ω_2 is the most relevant parameter from a physical point of view. It gives the transition frequency between the non-conducting (σ' α ω) and the conducting (σ' = cte) behaviour. The evolution of ω_2 as a function of Bioglass® concentration is reported in Table 1. In the two series of composite foams, the frequency transition ω_2 increased (the size of the conductivity plateau decreased) with increasing Bioglass® concentration. These values confirmed that ionic conductivity decreases when the Bioglass® content increases and that the evolution of the ionic conductivity with Bioglass® content is different for the low and the high molecular weight foam series.

Fig. 6. *Log-log plots of the rescaled conductivity (**σ'**) versus frequency for (a) PDLLA-LMW and (b) PDLLA-HMW foams unfilled and filled with different concentrations of Bioglass .*

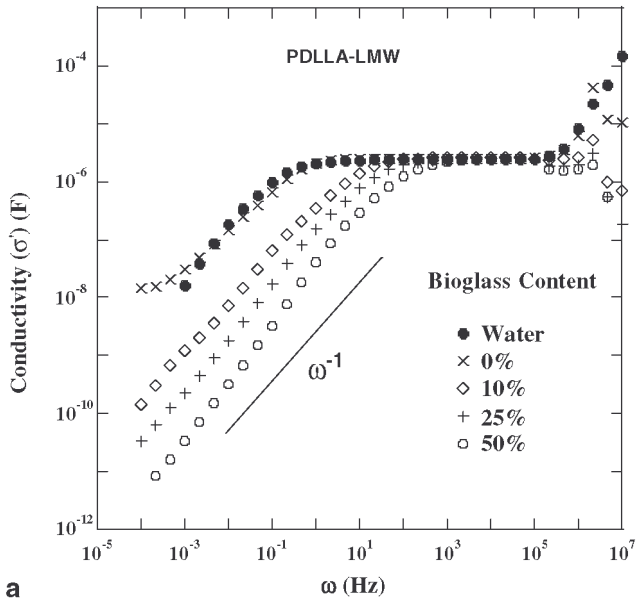

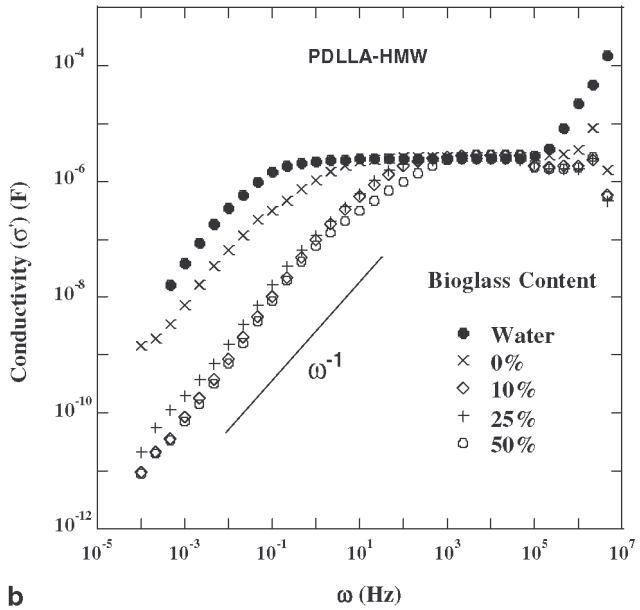

***Table 1**: Values of the transition frequency between conducting and non-conducting behaviour (ω_2) in hertz, for deionized water and water-impregnated* polymer/Bioglass composite foams

Deionized water	Polymer foams	Bioglass® content			
		0%	10%	25%	50%
0.15	PDLLA-LMW	0.24	8.12	22.06	83.34
	PDLLA-HMW	1.65	49.24	46.41	98.03

4. DISCUSSION

Morphological changes of TIPS-produced PDLLA/ Bioglass® composite foams with increasing concentration of Bioglass® particles (of mean particle size ≤ 5 μm) have been studied by image analysis and impedance spectroscopy. The histograms of pore orientations showed that in the absence of Bioglass®, the pores in PDLLA-HMW foams exhibit a more perfect orientation than in PDLLA-LMW foams. Moreover, these histograms showed that PDLLA-LMW foams without and with Bioglass®exhibit similar pore orientation, indicating that the addition of Bioglass® particles (up to 50 wt.%) did not influence pore morphology. On the contrary, for PDLLA-HMW foams, no significant difference in pore orientation was observed between neat and 10 wt.% Bioglass® filled foams whereas for higher Bioglass® content, pores became significantly less orientated.

In order to investigate the relation between pore morphological characteristics and pore connectivity, impedance spectroscopy measurements were performed. These measurements showed that for neat PDLLA-LMW foams, the interval of frequencies in which the ionic water conduction is constant was very close to that of deionized water. On the contrary, for composite foams containing 10-50 wt.% of Bioglass® , this interval decreased gradually. For PDLLA-HMW foams, impedance spectroscopy showed that, in comparison with reference water, the interval of frequencies in which the ionic water conduction is constant was significantly narrrower in the neat polymer foam and it was dramatically affected by the addition of Bioglass® particles. It can be therefore concluded that for all composites, whatever the Bioglass® content, the interval of frequencies in which ionic conduction arises was narrower than for the neat polymer foams, indicating that the addition of Bioglass hindered the free motion of the charge carriers as compared to the foams without Bioglass®.

A comparison between SEM observations and image analysis results, on one hand, and impedance spectroscopy measurements, on the other hand, suggests that the observed decrease of free motion of charge carriers upon addition of Bioglass® particles is not related to a loss of pore orientation. The loss of ionic conductivity can be attributed to an increase of the roughness of pore surfaces leading to an increased path tortuosity between pore channels. Moreover, for high Bioglass® content the smaller pores can be partially obstructed, hindering the charge carriers movement. This phenomenon, which can be observed at higher SEM magnifications than the one used for image analysis, is illustrated in Fig. 7.

***Fig. 7.** SEM micrographs of a PDLLA/Bioglass® composite foam with high concentration of Bioglass® particles (50 wt.%) at high magnification showing: (a) surface roughness and (b) pore obstruction.*

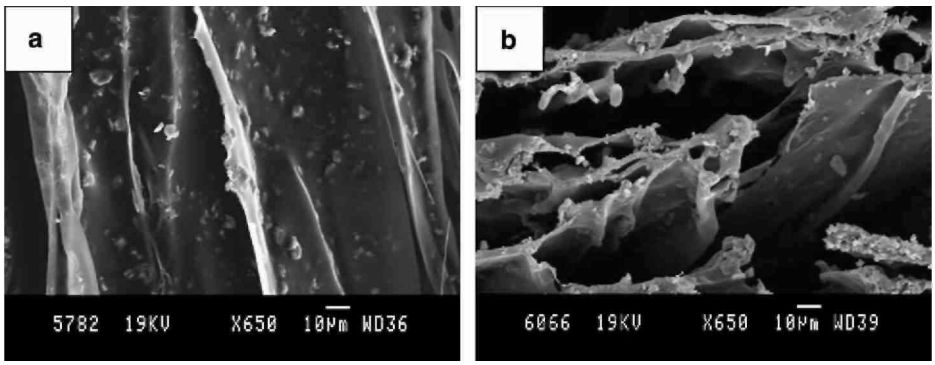

The different ionic conduction behaviour of PDLLA-LMW and PDDLA-HMW foams with addition of Bioglass® can be explained in terms of the porous structure. A small quantity of Bioglass® particles randomly dispersed in a poorly oriented and non-structured scaffold, such as the investigated PDLLA-LMW foams, can hardly obstruct the overall pore connectivity. Should a pore become blocked then the charge carriers could easily find a way for migration through neighboring pores. This explains the gradual evolution of the ionic conduction response of PDLLA-LMW foams upon increasing Bioglass® content. On the contrary, for the highly oriented and structured PDLLA-HMW foams, there are very few paths through which a charge carrier could move from

one point to another. Should these few paths be blocked by a small quantity of Bioglass® particles, a whole branch of the percolating pore structure could be obstructed. This should lead to a very steep response of the ionic conductivity to an increase of Bioglass® content as the motion of charge carriers becomes confined to small regions of the foam.

Overall, for PDLLA-LMW foams, Bioglass® content did not affect pore morphology but it decreased the pore connectivity. In the case of PDLLA-HMW foams, both pore morphology (orientation) and connectivity are changed upon addition of Bioglass® particles. However, while the inferior threshold of connectivity is reached already for a concentration of 10 wt.% Bioglass® , the addition of 20 wt.% Bioglass® is required to significantly affect pore orientation. Image analysis and impedance spectroscopy results showed that the connectivity of PDLLA-LMW composite foams is less sensitive to Bioglass® content than that of PDLLA-HMW foams, leading to a better control of pore connectivity. On the contrary, the pore orientation is more dependent on Bioglass® content in PDLLA-HMW foams (at least for up to 25 wt.% Bioglass® content). Both parameters, i.e., pore orientation and pore connectivity, are key features in the design of porous polymer scaffolds for tissue engineering applications. The results reported in this study indicate thus the suitability of the non-destructive characterization methods employed, image analysis and impedance spectroscopy, to quantitatively assess the effect of addition of Bioglass® particles on the pore structure of TIPS fabricated composite foam scaffolds.

5. CONCLUSIONS

SEM observations, image analysis and impedance spectroscopy have been used to characterize the morphology and the pore connectivity of PDLLA/Bioglass® foams prepared by TIPS. These characterization techniques showed for the first time in quantitative terms that pore connectivity of PDLLA-LMW and PDLLA-HMW composite foams is affected by the addition of Bioglass® particles. These particles do not affect the pore orientation of PDLLA-LMW foams whereas at a concentration of 25 wt.% Bioglass , they significantly decrease the pore orientation of PDLLA-HMW foams. The findings of this investigation are relevant considering the design of composite PDLLA/Bioglass® scaffolds of tailored porosity for bone tissue engineering, which is the subject of on-going investigations.

Acknowledgements

S.B. is indebted to Action de Recherche Concertée (ARC No. 00/05-265) for financial support. V.M. is ''Postdoctoral Researcher'' by the Fonds National de la Recherche Scientifique (FNRS) and is indebted to FNRS for financially supporting her post-doc stay at Imperial College London. CERM is indebted to the ''Services Federaux des Affaires Scientifiques, Techniques et Culturelles'' for support in the frame of the ''Poles d'Attraction Interuniversitaires: PAI 5/03''.

References

[1] Langer R, Vacanti JP. Tissue engineering. Science 1993;260(5110):920-6.
[2] Hutmacher DW. Scaffolds in tissue engineering bone and cartilage. Biomaterials 2001;21:2529-43.
[3] Maquet V, Blacher S, Pirard JP, Jérôme R. Characterization of porous polylactide foams by image analysis and impedance spectroscopy. Langmuir 2000;16(26):10463-70.
[4] Blacher S, Maquet V, Schils F, Martin D, Schoenen J, Moonen G, et al. Image analysis of the axonal ingrowth into poly(D,L-lactide) porous scaffolds in relation to the 3-D porous structure. Biomaterials 2003;24:1033-40.
[5] Boccaccini AR, Maquet V. Bioresorbable and bioactive polymer/ Bioglass® composites with tailored pore structure for tissue engineering applications. Comp Sci Technol 2003;63:2417-29.
[6] Hench LL, Splinter RJ, Allen WC, Greenlee TK. Bonding mechanisms at the interface of ceramic prosthetic materials. J Biomed Mater Res 1971;2:117–41.
[7] Maquet V, Boccaccini AR, Pravata L, Nothinger I, Jérôme R. Porous poly(alpha-hydroxyacid)/Bioglass® composite scaffolds for bone tissue engineering. I: Preparation and in vitro characterisation. Biomaterials 2004;25:4185-94.
[8] Coster M, Chermant J. Précis d'analyse d'images. Paris: CNRS; 1985.
[9] Hilfer R. Geometric and dielectric characterisation of porous media. Phys Rev B 1991;44:60-75.
[10] Pissis P, Anagnostopolou-Konsta A, Apekis L, Daoukaki-Dia-manti D, Christodoulides C. Dielectric effects of water in water-containing systems. J Non-Cryst Solids 1991;131:1174-81.
[11] Pissis P, Laudat J, Daoukaki D, Kyritsis A. Dynamic properties of water in porous Vycor glass studied by dielectric techniques. J Non-Cryst Solids 1994;171:201-7.
[12] Gutina A, Axelrod E, Puzenko A, Rysiakiewitz-Pasek A, Kozlo-vich N, Feldman Y. Dielectric relaxation of porous glasses. J Non-Cryst Solids 1998;235-237:302-7.
[13] Cole KS, Cole RH. Dispersion and absorption in dielectrics. I: Alternating-current characteristics. J Chem Phys 1941;9:341–51.
[14] Debye P. Polar molecules. New York: Chemical Catalog Co.; 1929.
[15] Davidson DW, Cole RH. Dielectric relaxation in glycerol. J Chem Phys 1950;18:1417.
[16] Havriliak S, Negami JS. Complex plane analysis of a-dispersions in some polymer systems. J Polym Sci, Polym Symp 1966;14:99–103.
[17] Williams G, Watts DC. Non-symmetrical dielectric relaxation behaviour arising from a simple empirical decay function. Trans Faraday Soc 1970;66:80–5.
[18] Dissado LA, Hill RM. A cluster approach to the structure of imperfect materials and their relaxation spectroscopy. Proc Roy Soc A 1983;390:131–80.
[19] Jonscher AK. Physical basis of dielectric loss. Nature (London, United Kingdom) 1975;253(5494):717–9.